

**VARIATIONS IN APPARENT SURFACE TEMPERATURE AS A FUNCTION OF IMAGER VIEWING
ANGLE**

by

Melissa Ann Stewart

A thesis submitted to the Faculty of the University of Delaware in partial fulfillment of the requirements for the degree of Bachelor of Civil Engineering with Distinction.

Spring 2010

Copyright 2010 Melissa Stewart

All Rights Reserved

**VARIATIONS IN APPARENT SURFACE TEMPERATURE AS A FUNCTION OF IMAGER VIEWING
ANGLE**

by

Melissa Ann Stewart

Approved: _____
Jack A. Puleo, Ph.D.
Professor in charge of thesis on behalf of the Advisory Committee

Approved: _____
Thomas McKenna, Ph.D.
Committee member from the Department of Geological Sciences

Approved: _____
Christopher Meehan, Ph.D.
Committee member from the Department of Civil and Env. Engineering

Approved: _____
James Glancey, Ph.D.
Committee member from the Board of Senior Thesis Readers

Approved: _____
Ismat Shah, Ph.D.
Chair of the University Committee on Student and Faculty Honors

ACKNOWLEDGMENTS

First and foremost I need to thank my thesis advisor, Jack Puleo, for his endless support and unwavering confidence in my ability to complete this project. I would also like to thank Tom McKenna and Tim Sliwinski for their incredible work ethic. Lastly, I need to thank the Undergraduate Research Program for giving me this amazing opportunity.

TABLE OF CONTENTS

LIST OF TABLES	vi
LIST OF FIGURES	vii
ABSTRACT	ix
Chapter	
INTRODUCTION	1
EQUIPMENT	5
2.1 Testing Apparatus.....	5
2.2 Imagers	7
2.2.1 Visible Spectrum: Red, Green, Blue (RGB)	8
2.2.2 Near Infrared (NIR).....	9
2.2.3 Long Wave Infrared (FLIR).....	13
2.3 Sensors	16
2.3.1 Campbell Scientific Data Collection System.....	17
2.3.2 Single-Point Infrared Thermometer	18
2.4 Temperature Reference Emitter	18
2.5 Hot plate	20
2.6 Mylar Reflectivity Panel.....	21
MATERIALS	23
3.1 Types of Sediment	23
PROCEDURES	26

4.1	Experiment	26
4.2	Analysis	27
RESULTS	28
5.1	Raw Data.....	28
DISCUSSION	31
6.1	A Discussion of Uncorrected Data.....	31
6.2	Sources of Error	32
6.2.1	Environmental	32
6.2.2	Sediment	32
6.2.3	Equipment.....	33
6.3	Corrected Data	34
CONCLUSIONS	37

LIST OF TABLES

Table 1.1:	Emissivity values for common materials	2
Table 2.1	Table of CamSci sensors used throughout experimentation and potential measurement error associated with each sensor within a reasonable temperature range.	17

LIST OF FIGURES

Figure 1.1:	Series of images taken with thermal imager showing an error in apparent surface temperature increasing with an increase in imager viewing angle.....	4
Figure 2.1:	Overall apparatus set-up with preliminary tank shown and three imagers mounted to secondary goniometer arm.	6
Figure 2.2:	Position plate at base of primary goniometer arm with position pin set at 50° from nadir.	6
Figure 2.3:	Imagers mounted to secondary goniometer arm.....	7
Figure 2.4:	Graphic of electromagnetic spectrum.	8
Figure 2.5:	Sony Model DFW X710 (RGB imager)	9
Figure 2.6:	Allied Vision Technologies: Guppy F-038C (NIR) with filter attached.....	10
Figure 2.7:	Graph of spectral response of NIR CCD.....	11
Figure 2.8:	Graph depicting transmittance for several different types of filters.	11
Figure 2.9:	The total system response between filter and lens is depicted in this graph by the red line	12
Figure 2.10:	RGB (top), NIR (middle), and LWIR (bottom) images taken at a nadir position.	13
Figure 2.11:	ThermaCAM model P45HSV, used to collect long-wave infrared experiment data.....	14
Figure 2.12:	Screen shots captured during analysis of thermal images using Researcher software.....	15

Figure 2.13:	Screen shots captured during analysis of thermal image using Researcher software.	16
Figure 2.14:	TRE without cover plate	19
Figure 2.15a:	Computer-rendered side view of Temperature Reference Emitter	19
Figure 2.15b:	Computer-rendered plan view of Temperature Reference Emitter.	20
Figure 2.16:	RGB image of sediment and TRE setup in experiment area	21
Figure 2.17:	Thermal (left) and RGB (right) images of the Mylar Reflectivity Panel.....	22
Figure 3.1:	Image of four different sediments tested.....	23
Figure 3.2:	Graphed results of mechanical sieve analysis completed on Fine Sand.....	24
Figure 3.3:	Graphed results of mechanical sieve analysis completed on Coarse Sand.....	25
Figure 5.1:	Graphs depict temperature plotted as a function of imager viewing angle for 45°C nominal temperature.	29
Figure 5.2:	Temperature as a function of imager viewing angle for TRE.....	30
Figure 6.1:	Difference between corrected FLIR and corrected IR temperature data for all sediments and temperature ranges.....	36

ABSTRACT

Remote sensing has the potential to be a useful tool for analyzing the physical properties and spatio-temporal variations of sediments in intertidal environments. In order for this goal to be achieved, we must first understand the behavior of these sediments under different environmental conditions, such as temperature and moisture content. A variety of remote sensors can have inherent errors as a function of viewing angle and the effect that parameters like sediment type and nominal temperature have on these errors. Thus, these effects must be quantified. In order to have control over the type of sediment and temperature of the samples being analyzed, we constructed a laboratory environment to explore the effect that imager viewing angle has on different sediments for five nominal temperature values. It is found that apparent temperature variations are only on the order of 1°C for imager angles with respect to nadir up to about 30 degrees. However, for larger angles, those more indicative of tower-based imager deployments, apparent temperature variations on the order of 4°C were observed. Variations in error for temperature as well as sediment type are also presented and discussed in this paper.

Chapter 1

INTRODUCTION

The determination of soil properties within inter-tidal environments using traditional soil testing methods poses a unique challenge. Testing must be done to determine trafficability in order to ensure the soil can sufficiently support testing equipment, but trafficability cannot be determined without first knowing basic soil properties. One potential method that could be used to determine these properties is remote sensing. However, the spatio-temporal instability of tidal flat properties is a major limitation for the development of robust remote sensing applications due to a number of factors that add variation to the remotely-acquired data. Some factors are contained within one complication affecting all thermal infrared imagers; the required use of an emissivity parameter to unambiguously estimate radiometric temperature.

Emissivity is a measure of a body's ability to absorb energy. A "black body" has an emissivity of 1.0, meaning all energy is absorbed and no energy is reflected. A material's emissivity is the ratio of energy radiated by that material to that of a black body under the same environmental conditions. Table 1.1 shows emissivity values for several common materials. Water has an emissivity of about 0.98, but can vary due to turbidity, salinity and water surface texture. Emissivity for thermal imagers is also strongly dependent on the angle with respect to the viewing surface. Figure 1.1 depicts a series of images taken with a thermal imager over an intertidal environment and makes clear the change in emissivity of water as imager viewing angle increases. The error in apparent surface temperature in this figure is approximately 6°C. For angles between 40° and 80° (similar to tower-based

applications) the emissivity of water can potentially decrease to between 0.55 and 0.77 (Buettner and Kern, 1965).

Table 1.1: Emissivity values for common materials. In a test involving the Aluminum and the Black Body at the same temperature, the Black Body would absorb 100% of the energy, while the Aluminum would absorb only 4%, reflecting the remaining 96%.

Material	Emissivity
Black Body	1.0
Water	0.98
Concrete	0.92
Wrought Iron	0.28
Aluminum	0.04

Like water, sediment emissivity can vary significantly. Before attempting to quantify physical properties of intertidal environments using remote sensing, we need to be able to quantify the potential error due to imager viewing angle for a variety of temperature ranges and sediment types. Extensive field work in this area has been undertaken (e.g. Cuenca and Sobrino; 1999, 2004, 2005). A vast majority of these experiments involved using radiometers to obtain surface radiation data and the use of a constant-radius, variable-angle testing apparatus most commonly referred to as a Goniometer. While these previous works have laid down the foundation for future work by mapping out trends and establishing the need for additional research, they have all been performed in the field with little or no

control over temperature. Also, the sediment types analyzed were limited to in-situ soils available in the immediate testing area.

Our research brings the same theory applied during field testing into a lab setting, where parameters like sediment type, sediment temperature, and ambient environmental conditions are more easily controlled. Although there is more opportunity in a laboratory setting to control ambient conditions, there is still error in data collected due to the environmentally sensitive nature of thermal experimentation. In this work, I will be looking at four significantly different sediment types at six different temperature ranges. Raw data for all experiments will be presented as well as data that has been corrected for any quantifiable error encountered throughout the experiments.

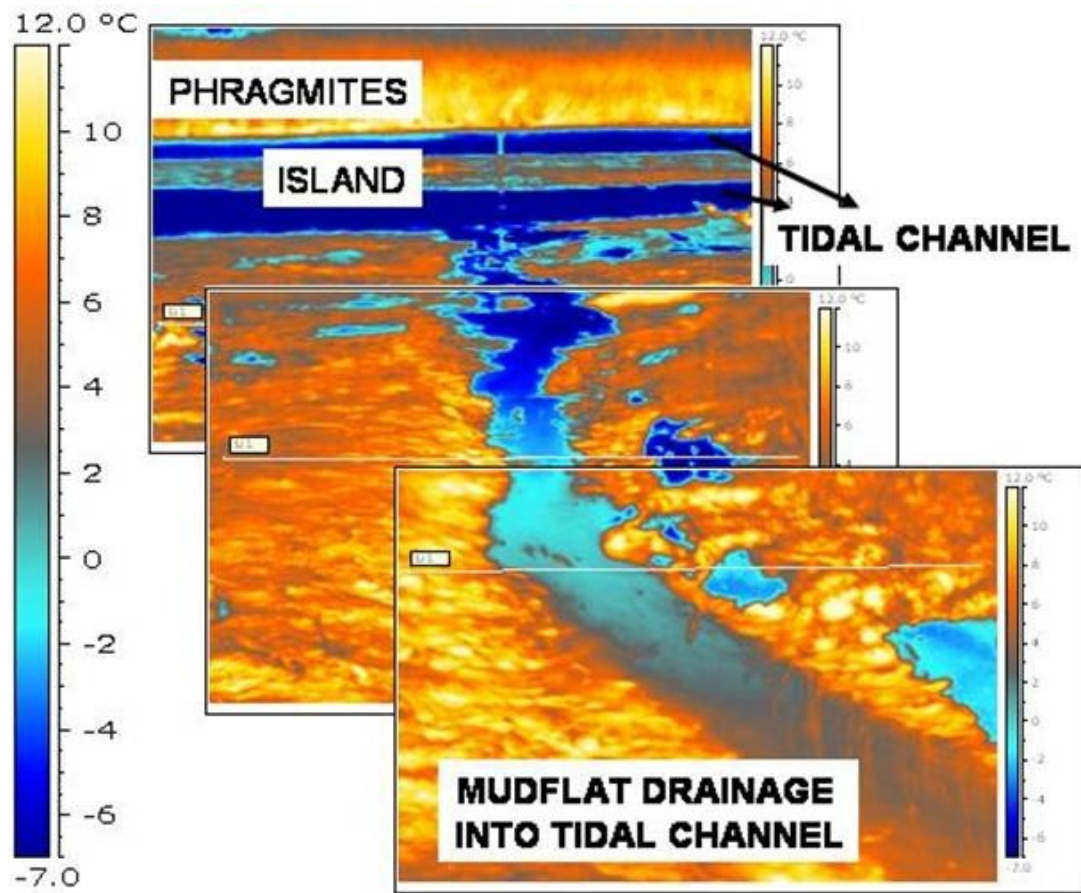


Figure 1.1: Series of images taken with thermal imager showing an error in apparent surface temperature increasing with an increase in imager viewing angle. The dark blue areas indicate a surface temperature reading of approximately -6°C , while the water closest to the camera (at the smallest viewing angle) reads at a more reasonable 4°C .

Chapter 2

EQUIPMENT

2.1 Testing Apparatus

In order to fulfill the need for a multi-angle, constant-radius testing apparatus, a goniometer was fabricated from aluminum, attached to a solid foundation, and centered over the testing area. Figure 2.1 is an image of the overall goniometer setup. The tank seen in the viewing area was used for preliminary experiments whose results were inconclusive, though they proved helpful in exploring the accuracy of the apparatus and testing many of the sensors (discussed in Section 3) used in the actual experiment. Also visible in this image is some of the insulation used to isolate the testing area from radiation and reflection from the apparatus and hardware located behind the primary goniometer arm, as discussed in section 5.2 of this paper.

The primary radius arm was attached to an aluminum plate at the foundation with pin positions in 5° increments at 85° from the vertical position from either side of nadir. Figure 2.2 shows the base of the primary arm as attached to the plate with position pin set at 50° from the nadir position.



Figure 2.1: Overall apparatus set-up with preliminary tank shown and three imagers mounted to secondary goniometer arm.

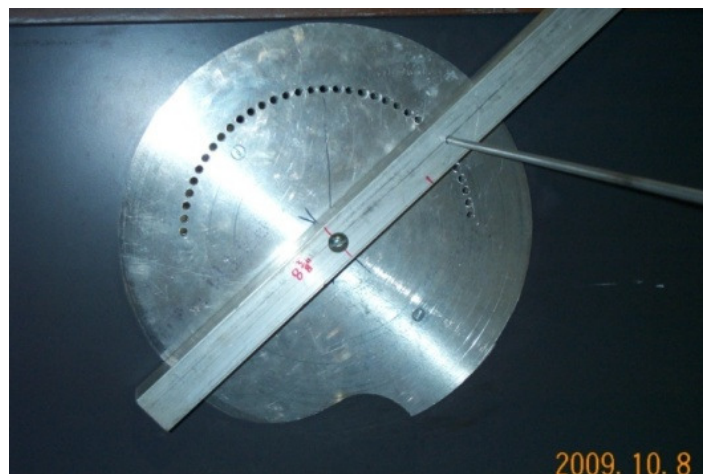


Figure 2.2: Position plate at base of primary goniometer arm with position pin set at 50° from nadir.

The secondary arm was positioned at 3.3 meters from the pivot point to allow for full view of the testing area for all imagers used in the experiment. Imagery was mounted approximately 1 meter from the primary arm and centered over the testing area. Imagery was attached to the secondary arm with all lenses centered 0.3 meters below the secondary arm. Figure 2.3 shows all three imagers attached to the secondary goniometer arm at an angular position of 75° from nadir.



Figure 2.3: Imagery mounted to secondary goniometer arm. From left to right: Thermal Imager, RGB Imager, and NIR Imager (discussed in section 2.2).

2.2 Imagery

Three different imagers were used for this study: visible (RGB), near infrared (NIR), and thermal infrared (FLIR). Three imagers were chosen to ensure that a wide range of

the electromagnetic spectrum could be collected. Figure 5.4 shows a graphic of the electromagnetic spectrum and shows where wavelengths analyzed in this study fall along the spectrum.

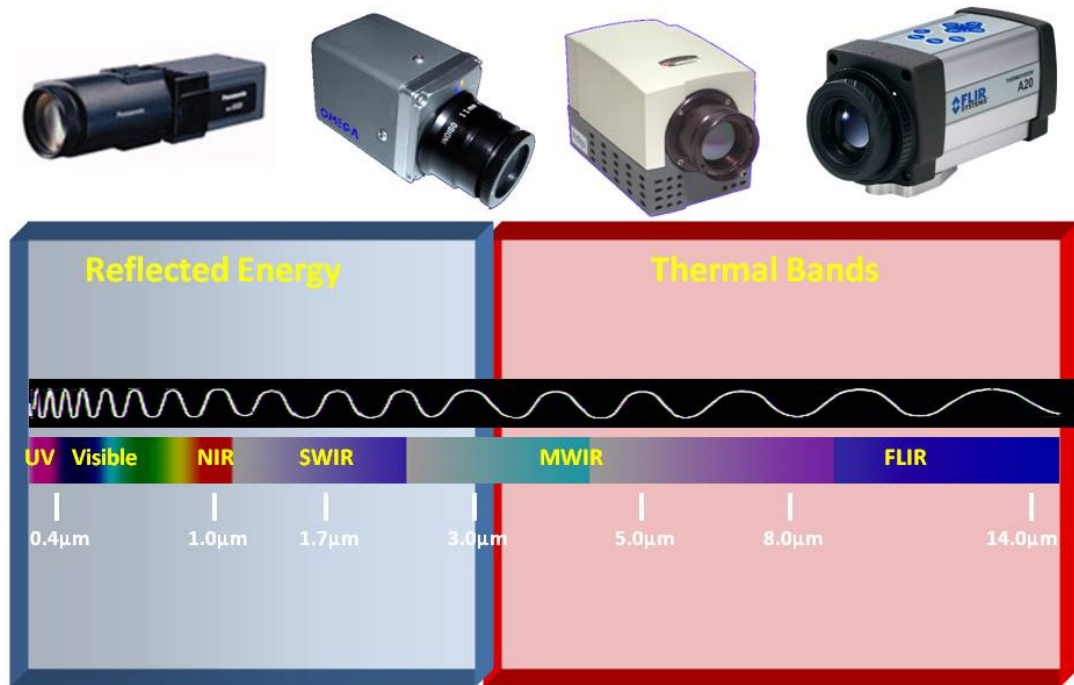


Figure 2.4: Graphic of electromagnetic spectrum. Visible and near infrared waves were analyzed within the reflected end of the spectrum, with long wave infrared waves studied within the thermal bands.

2.2.1 Visible Spectrum: Red, Green, Blue (RGB)

The imager used to collect visible spectrum data was a Sony Model DFW X710 (see Figure 2.5). The imager uses a 1/3" Progressive Scan IT CCD with 1,034 x 779 pixels. Images were used to verify the conditions of the testing area and to cross-check against FLIR

and NIR images. The Fire-i 1394 Camera Control Application was utilized to collect RGB images and control imager properties such as exposure and shutter speed.



Figure 2.5: Sony Model DFW X710 (RGB imager)

2.2.2 Near Infrared (NIR)

The NIR imager is a Guppy F-038C manufactured by Allied Vision Technologies (see Figure 2.6). AVT Smartview software was used to collect images and specify imager properties. The imager uses a $\frac{1}{2}$ " Sony interlaced CCD with 752 x 580 pixels. The CCD has a spectral response that spans the visible and NIR ranges (Figure 2.7). However, our interest is to remove as much of the response in the visible band as possible. To achieve this, an X-Nite 665 filter with a cut off frequency of 625 nm (Figure 2.8) was placed on the imager lens. The total system response can be seen in Figure 2.9, which shows the response of the CCD

alongside the response of the filter and also depicts the combination of the two. The total system response within the strictly NIR wavelengths was not strong enough to overcome experimental error, therefore the data collected from the NIR imager was not analyzed for this project.



Figure 2.6: Allied Vision Technologies: Guppy F-038C (NIR) with filter attached

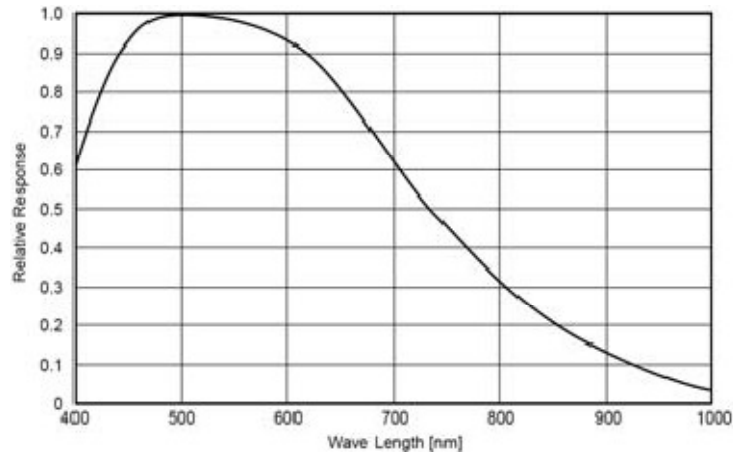


Figure 2.7: Graph of spectral response of NIR CCD. Note that the lens response spans both the visible and NIR spectrum, and therefore a filter must be used to control the energy that passes through to the lens in order to isolate a smaller range of wavelengths.

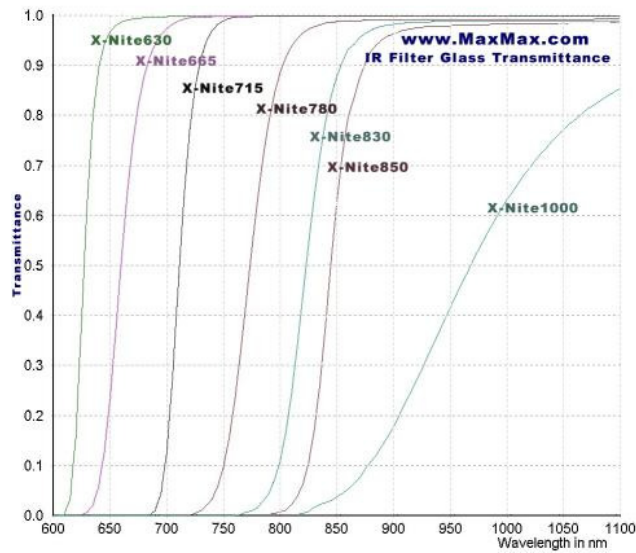


Figure 2.8: Graph depicting transmittance for several different types of filters. For this study, an X-Nite665 was used which has a cut-off frequency of 625 nm (or 50% at 650 nm).

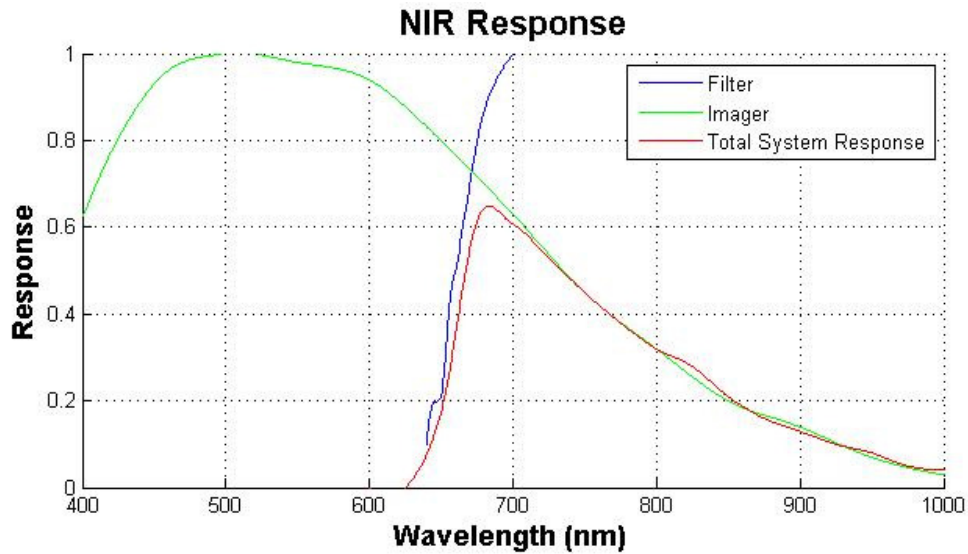


Figure 2.9: The total system response between filter and lens is depicted in this graph by the red line. The limited total system response for the NIR bands can be seen in this graph and was not strong enough to warrant analysis in this project.

Figure 2.10 shows an example NIR image taken from the nadir position alongside images taken with the visible and thermal imagers. These images show the limited data that was available from the NIR imager, and further verifies that the NIR data was not sufficient enough to warrant analysis during the course of this project.

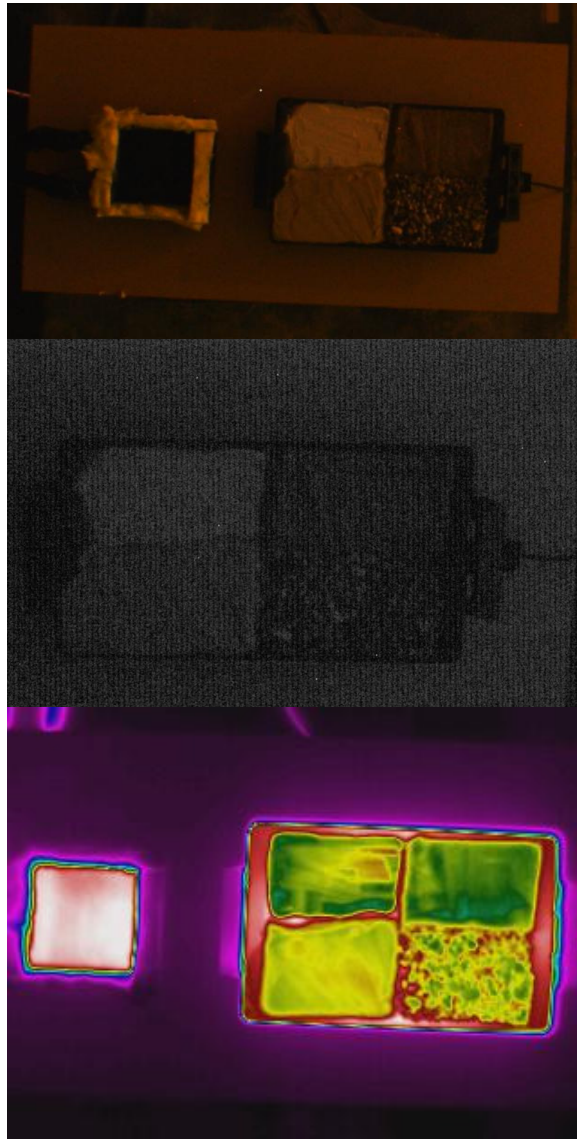


Figure 2.10: RGB (top), NIR (middle), and LWIR (bottom) images taken at a nadir position.

2.2.3 Long Wave Infrared (FLIR)

The thermal imager used for this project was a ThermaCAM model P45HSV (see Figure 2.11). This imager uses a focal plane array (FPA) uncooled microbolometer with 320x240 pixels. A 36mm focal length lens with a 14°x19° field of view, 7.5 to 13um spectral range, and a 1.1 mrad spatial resolution. The FLIR has a thermal sensitivity of 0.05°C at 30°C. The software used for analysis of thermal images was ThermaCAM Researcher version 2.9. The program was used to determine minimum, maximum, mean, and point value data from each image. Figure 2.12 contains screen shots from two different analyses of thermal images using the Researcher software. The areas used to determine mean data values is clearly visible in both images, as is the area where single-point data was taken.



Figure 2.11: ThermaCAM model P45HSV, used to collect long-wave infrared experiment data.

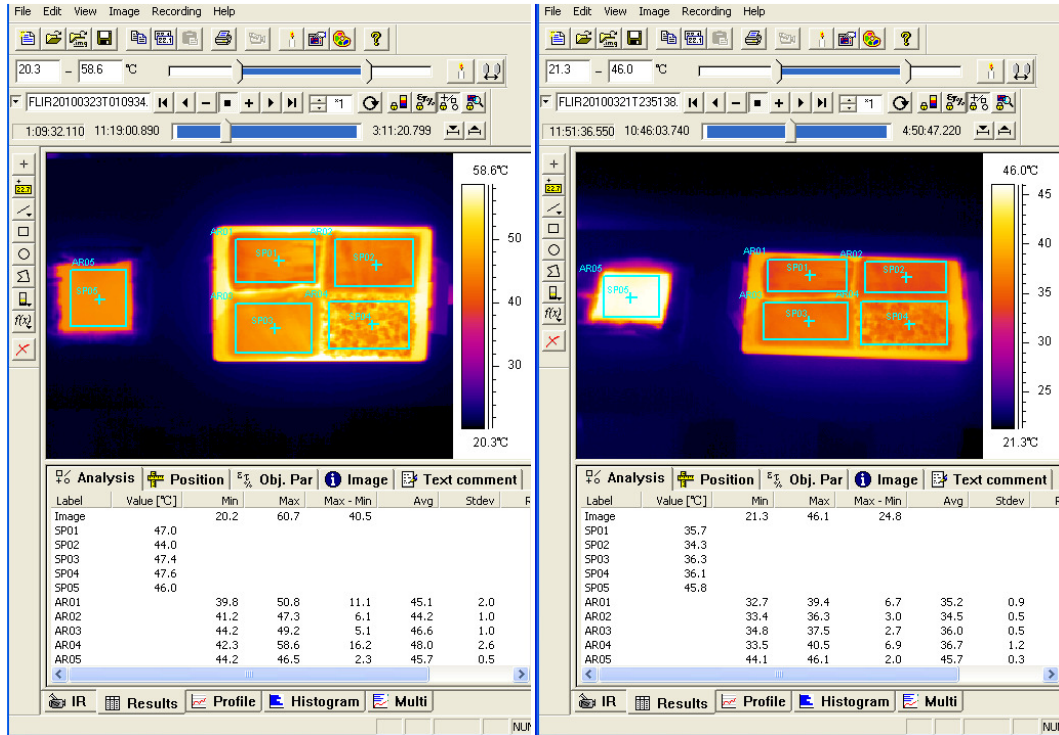


Figure 2.12: Screen shots captured during analysis of thermal images using Researcher software. The image on the left was an analysis of an image taken at nadir, and the image on the right was an analysis of an image taken at 30° from nadir. In each image, the Temperature Reference Emitter (see Section 2.4) is seen on the left with the hot plate containing 4 sediments to the right.

Figure 2.13 is a larger view of the image on the left in Figure 2.13 with the analysis points and boxes removed for clarity. Easily seen in this image are edge effects and spatial variations in surface temperature. The latter of the two is due to surface roughness, heterogeneity of sediment surfaces, spatio-temporal variability on the surface of the hot

plate, and varying emissivity between soil types that shows as a variable surface temperature due to an emissivity of 0.96 being entered into the FLIR for all sediments.

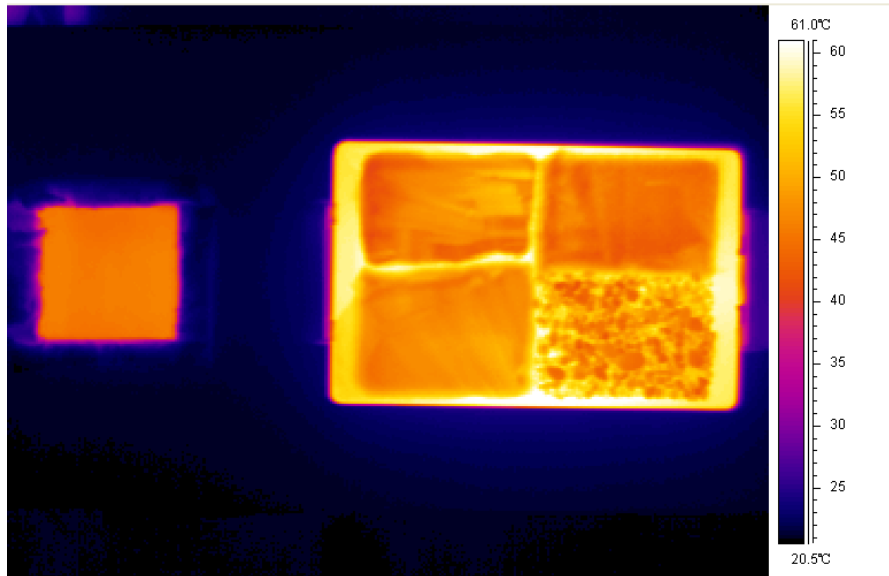


Figure 2.13: Screen shots captured during analysis of thermal image using Researcher software. Visible in this image are edge effects between each sediment (right side of image) and variations in temperature due to surface roughness, heterogeneity of sediment surfaces, spatio-temporal variability on surface of hot plate, and variable emissivity as a function of sediment type.

2.3 Sensors

A variety of sensors were used to collect a multitude of data throughout experimentation. Monitoring test samples throughout the experiment was a necessity, but

Careful consideration of ambient conditions was also necessary in order to understand better the driving forces behind unexpected changes in the testing environment and subsequent effects on experimental data.

2.3.1 Campbell Scientific Data Collection System

Due to the sheer number of data points needed to be collected during experimentation, a Campbell Scientific CR1000 Measurement and Control System (CamSci) was acquired, along with a multitude of sensors from a variety of manufacturers to be used with the logger. Table 2.1 lists the sensors used in this experiment as well as potential error associated with each device.

Table 2.1 Table of CamSci sensors used throughout experimentation and potential measurement error associated with each sensor within a reasonable temperature range. Note: SM200 and NR01 used for preliminary experiments only.

Data Collected	Sensor ID	Error	Manufacturer
Temperature	TM10	0.5°C	Dynamax
Air Temperature	HMP50	0.4°C	Campbell Scientific, Inc
Relative Humidity	HMP50	0.5%	Campbell Scientific, Inc
Soil Moisture	SM200	3%	Delta-T Devices Ltd
Ambient Short Wave and Long Wave Radiation	NR01	5%	Hukseflux

The software used with this system was PC400 version 4.0 Datalogger Support Software. This program was used to monitor sensors real-time, collect data points at predetermined intervals, and export data tables in CSV format for further analysis. The software logged both single-point data values and also averages over a predetermined period of time (2 minutes for this experiment).

2.3.2 Single-Point Infrared Thermometer

During the course of experiments a Fluke brand single-point Infrared thermometer with a distance to spot size ratio of 12:1 was used to determine sediment temperature at each goniometer arm position. Measurements were taken at nadir and at a constant distance from the sediment in approximately the same area of sediment. Variation in surface roughness and possible edge effects were taken into consideration when determining approximate area of IR temperature measurement.

2.4 Temperature Reference Emitter

Due to the variations in temperature ranges and IR temperature measurements, we established a need for a constant temperature reference in all thermal images. We fabricated a Temperature Reference Emitter (TRE) to ensure a constant value for all arm angles (see Figures 2.13 and 2.14).

The TRE was fabricated from a solid piece of copper with a channel machined into the material that doubled back on itself to minimize temperature variability throughout the system. It was heavily insulated and attached to a water bath (see Figure 2.13) set at a constant temperature, which was monitored by a mercury thermometer as well as a TM10 sensor inserted approximately 2 cm into the solid copper face of the TRE.

After being insulated and fitted with a TM10 sensor to monitor internal temperature, the TRE was painted with Krylon paint of a known emissivity to ensure a constant surface emissivity and minimize variations caused by minor imperfection in the surface.



Figure 2.14: TRE without cover plate (left); TRE covered, painted, and insulated (center); water bath (right).

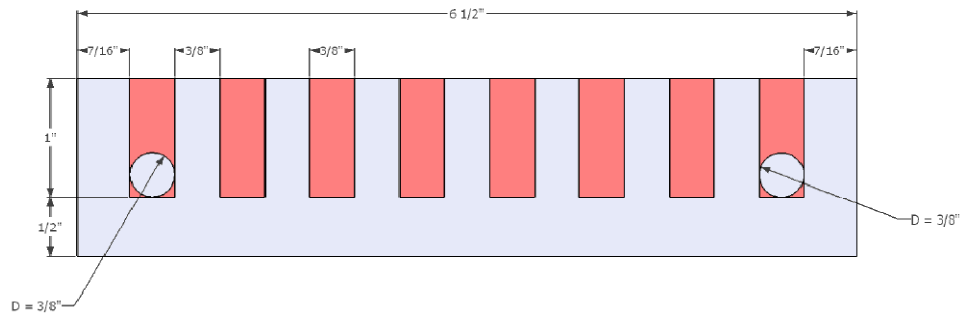


Figure 2.15a: Computer-rendered side view of Temperature Reference Emitter. Red areas indicate channel milled into copper and blue areas represent solid copper (opening for TM10 temperature sensor not shown).

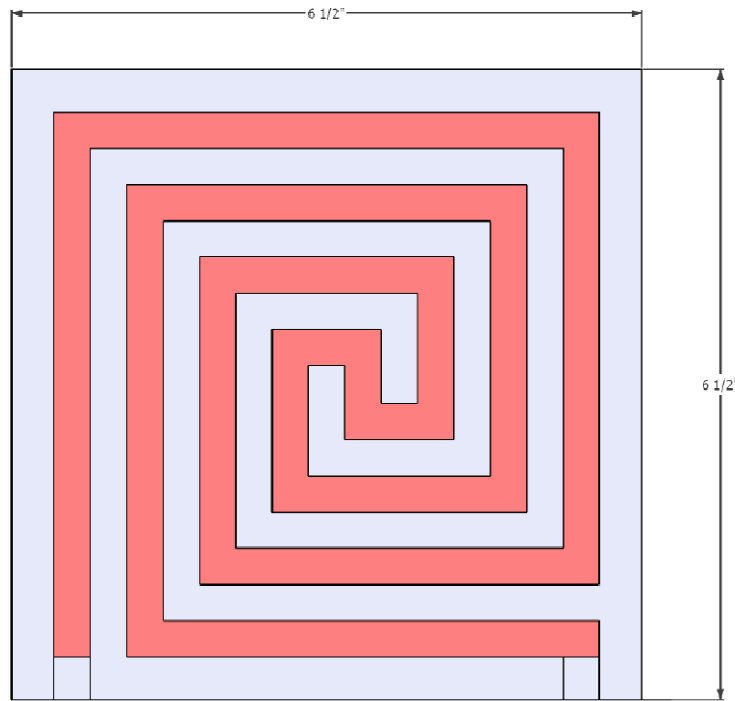


Figure 2.15b: Computer-rendered plan view of Temperature Reference Emitter. Red areas indicate channel milled into copper and blue areas represent solid copper.

2.5 Hot plate

The need was established early on for a heat source which could accommodate several samples and maintain a relatively constant temperature within a reasonable temperature range. Preliminary experiments were done on several different hot plates to determine which of those available to us could establish several constant temperature ranges between ambient air temperature and 50°C with the least amount of spatio-temporal

variation. Figure 2.16 shows the hot plate chosen with all four sediments arranged on it. Although this hot plate had smallest magnitude of spatio-temporal variation, there was still some error associated with it which is discussed at length in Chapter 6. Most notable was a slight temporal variation of around 3°C.



Figure 2.16: RGB image of sediment and TRE setup in experiment area. In this image, the hot plate can be seen (right side of image) with all 4 sediments in testing position. The TRE can also be seen to the left of this image. This TRE was insulated to avoid edge effects along the left side of the hot plate.

2.6 Mylar Reflectivity Panel

As discussed in previous sections, reflected energy within the testing area needed to be quantified throughout experimentation. This was accomplished by placing a metallized Mylar covered panel into the testing area and recording a thermal image at the

nadir position. With an emissivity close to zero, metallized Mylar reflects a vast majority of radiation within the environment, including infrared. To ensure all radiation from machinery and materials in the vicinity of the experiment would be reflected up to the thermal imager, the Mylar was wrinkled to allow for an adequate range of reflection angles. Figure 2.16 is an image of the Mylar Reflectivity Panel in position and a thermal image of the same set-up at nadir.

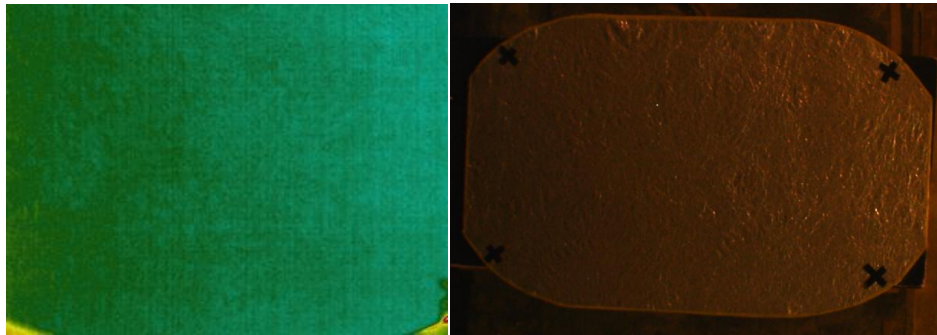


Figure 2.17: Thermal (left) and RGB (right) images of the Mylar Reflectivity Panel. The thermal image shows very little variability in temperature across the surface of the panel. This homogeneity was due, in part, to insulation placed between the testing area and the hardware needed for data collection.

Chapter 3

MATERIALS

3.1 Types of Sediment

Four different sediments were used for this project. The first was a sample of Kaolinite. The second was a poorly-graded Coarse Sand. The third sample is a well-graded Fine Sand. The remaining sample analyzed was Gravel. Figure 3.1 is an image of all four sediments as arranged on the hot plate during lab experiments. Sieve analysis data for the two different sand samples can be seen in figures 3.2, 3.4. These analyses were done to show the significant difference between the particle size distributions of the two different sediments. **The median diameter of the ... was ... and while the median diam of the ... was ... can also add sorting values.**



Figure 3.1: Image of four different sediments tested (starting from top left, clockwise): Kaolinite, Coarse Sand, Gravel, and Fine Sand.

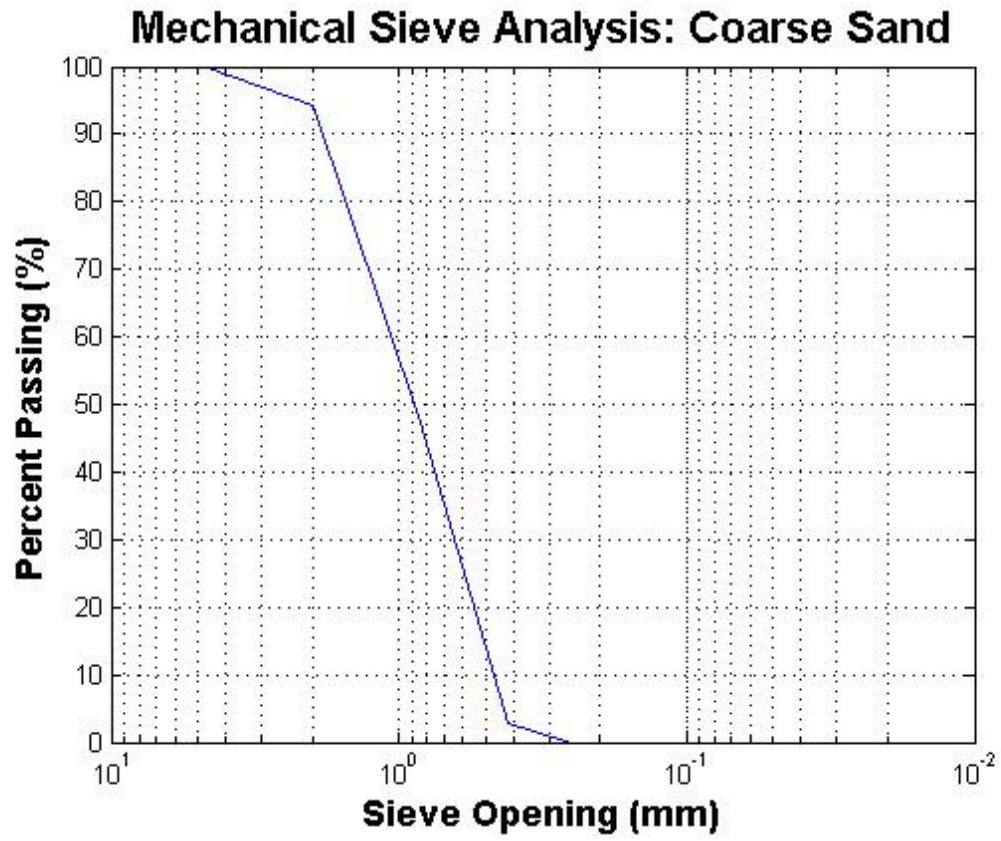


Figure 3.3: Graphed results of mechanical sieve analysis completed on Coarse Sand.

Chapter 4

PROCEDURES

4.1 Experiment

A rigorous testing procedure was established to ensure uniformity of data collection and to minimize variation from one hot plate setting and goniometer position to another. The first part of the procedure was set-up for experimentation. Due to the thermal sensitivity of the experiments, a majority of this procedure involved noting weather conditions and ambient lab conditions. Another important set-up component was collection of reflectivity data using FLIR images and a Mylar board placed within the test area. This data was later used to back out reflected energy due to the testing environment and isolate energy within the experiment.

Once set-up was complete, the next step was moving the primary goniometer arm into position and leveling both the primary and secondary arm. Insulation boards were placed between the desk containing computer and data logger before any images were taken to minimize thermal noise from nearby electronics. Once images were recorded for all three imagers and CamSci data was saved, the temperature of sediments and TRE were recorded using the IR thermometer at nadir approximately 2 cm from the surface.

This process was repeated for each position ranging from 15° from the horizontal to 165°, with two additional readings at the nadir position at the beginning and end of the experiment set. Six different temperature ranges were tested beginning with no external heat source through the high 40°C range. These temperature ranges are hereafter

identified by the nominal temperature around which the heat source oscillated: 28°C, 34°C, 30°C, 35°C, and 45°C.

4.2 Analysis

Thermal images obtained with FLIR were imported into ThermaCAM Researcher where minimum, maximum, mean, and standard deviation data were collected. In order to minimize edge effects, the area of analysis for each sediment type was reduced to the approximate center of the sample, ignoring the outside 2 – 3 cm of sample. In addition to collecting data over the average of individual samples, a point value was taken at the center of each sample in the images, comparable to the approximate area where the IR thermometer measurement was taken during experimentation.

Chapter 5

RESULTS

5.1 Raw Data

Plots of data collected for the 45°C nominal temperature show a clear trend in apparent surface temperature as a function of viewing angle (Figure 5.1). This general trend agrees with similar work performed in an outdoor environment (Cuenca and Sobrino, 2004), with little significant difference from 0° to 30° and the most dramatic difference seen with the largest viewing angle. Although there is a range of temperatures apparent when comparing one sediment to another, the trend seen for all sediments remains constant. This trend is most easily seen in Figure 5.2, which shows temperature as a function of camera viewing angle for the TRE.

In Figure 5.2, all four graphs are plotted on the same scale. This allows for an easy view of how sediment temperature varies from one sediment to another. The Coarse Sand and Kaolinite both obtained a temperature of approximately 45°C, while the Fine Sand reached a temperature of around 47.5°C. The Gravel held the most heat, reaching an average temperature according to the FLIR of 48°C. These differences are most likely due to varying thermal properties relative to the other sediments examined. These variations are a function of both the size and chemical make-up of the sediments, as well as physical properties like moisture content and porosity.

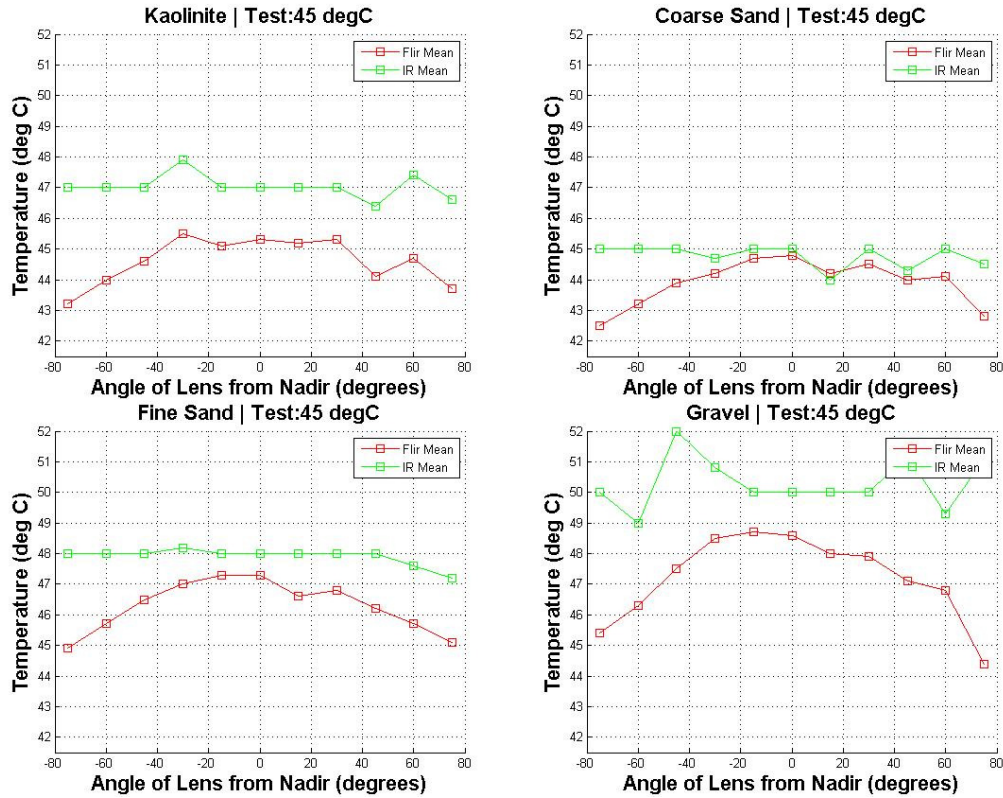


Figure 5.1: Graphs depict temperature plotted as a function of imager viewing angle for 45°C nominal temperature. Mean and point FLIR values are shown as well as average IR temperature measurement for each sediment type. Although the sediment data is not as consistent as the TRE data, the same trend can be seen; with the most significant error seen at a viewing angle greater than 30° from nadir.

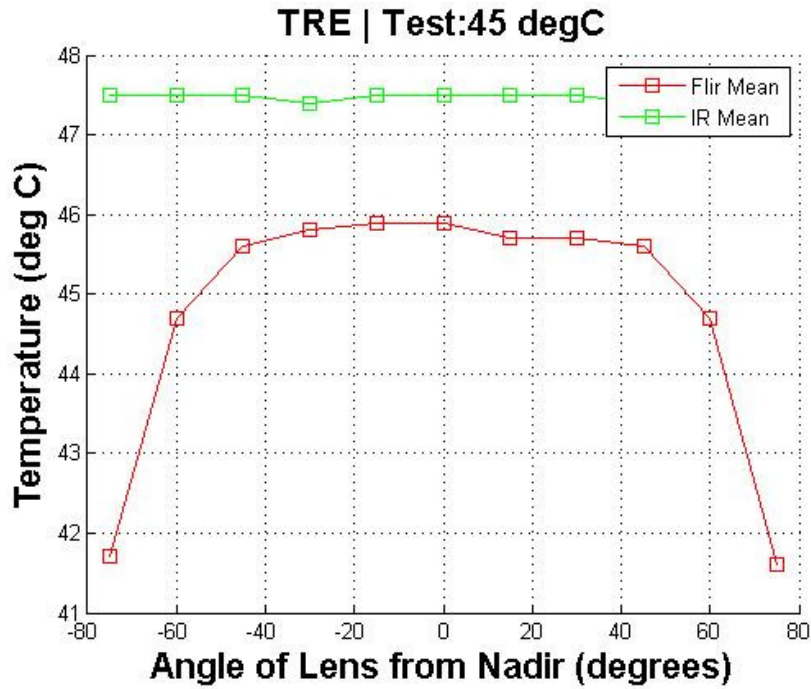


Figure 5.2: Temperature as a function of imager viewing angle for TRE. Mean FLIR values are shown, as well as mean IR temperature. The expected trend is clearly seen in this figure, with the most significant error at a viewing angle greater than 30° from nadir while the IR temperature reading remains reasonably constant.

Chapter 6

DISCUSSION

6.1 A Discussion of Uncorrected Data

Figure 5.2 shows raw data collected for the 45°C nominal temperature range. As stated in the previous section, the trend seen for all four sediments concurs with the trend seen for TRE data and in previous research done in the field. There are, however, several variations in temperature between sediment types that should be noted.

While all four sediments do show the expected trend, the data collected for the coarse and fine sands appears to have less variation throughout the experiment set than the other two samples. This is due to less error in data collected from these samples as discussed in detail in this chapter. A majority of the error came from surface roughness (Kaolinite, Gravel) and surface heterogeneity issues (Gravel). Also, the Kaolinite and sand samples were relatively homogeneous in terms of particle size distribution and volume of air voids, whereas the Gravel sample was heterogeneous throughout.

Also worth noticing are the variations in sediment temperature for each of the samples. There is as much as a 5°C difference in maximum temperature between the different samples. This is due, in part, to spatial variability in temperature across the surface of the hot plate. Another source of this difference is varying thermal properties for each sample.

6.2 Sources of Error

Although attempts were made throughout the experiment to identify potential sources of error and reduce their effect on the data collected, some error could not be avoided. In these cases attempts were made to quantify them and address their impact. These sources of error are able to be broken down into 3 major categories: Environmental, Materials, and Equipment.

6.2.1 Environmental

Thermal imagers work by collecting data on radiant energy and converting it to a temperature value by applying a known emissivity. Radiant energy is the sum of both emission and reflection for a given object. It is because of this that isolation of thermal testing environments plays such a critical role when working with thermal imagers. As mentioned in Chapter 2, ambient reflected energy was measured using a Mylar panel before and after each experiment set. Also a concern was that hardware necessary for data collection would provide an unaccounted-for heat source that would create a temperature gradient across the testing area which would later need to be quantified.

In order to minimize thermal noise, the testing area was well-insulated from hardware in the immediate area. The aluminum goniometer arm was also insulated to reduce reflection into the imager field of view.

6.2.2 Sediment

As shown in work done by Cuenca and Sobrino (2005), surface geometry plays a large part in how accurately radiant temperature can be measured. Both the Basin Sand and Coarse Sand samples show much less variability in temperature data collected with the IR

thermometer than the Kaolinite and Gravel samples. This is because of a relatively small surface heterogeneity compared with measurement spot size. The large particle sizes present in the gravel made it difficult to obtain a measurement that was indicative of the sample as a whole. On the other end of the spectrum, the small particle size present in the Kaolinite made it difficult to obtain a flat surface, so data collected with the IR thermometer often contained angular reflectivity present due to surface roughness.

6.2.3 Equipment

Hot Plate:

Although the size of the hot plate used was ideal for this experiment, allowing all four sediments to be heated by one source, there was temporal instability present in the form of fluctuations through each experiment set. The magnitude of this fluctuation remained approximately +/- 3°C throughout the experiment, with the length of the cycle largely dependent on temperature range. This is potentially due to an internal setting within the plate set to trigger at a given temperature difference. At higher temperatures (relative to ambient temperature), the plate cooled faster and therefore had a smaller cycle length. Inversely, at temperatures closer to ambient air temperature the plate did not cool as quickly and the cycle length of the fluctuation was larger. Temporal fluctuations within the 5-10 minute period of data collection were not quantified for this experiment and error due to this effect remains in the corrected data.

Single-Point Infrared Thermometer:

In an attempt to obtain consistent IR temperature measurements, data were collected using a consistent measurement procedure in same general area of each sediment

for each experiment set. However, there is still the potential for human error in the manner that temperature data was collected. In addition to this error, there was also a small amount of time that elapsed between when the FLIR image was taken and when IR data was recorded. Each goniometer arm position took approximately 5-10 minutes to complete, allowing for temperature fluctuation during data collection. The magnitude of this potential error depends on the length of the cycle of temporal fluctuations with the heat source.

FLIR:

Although there was as much as a 2°C error in temperature measured by the FLIR, this error was corrected using the TRE and CamSci data as noted in the next section.

6.3 Corrected Data

Raw data was corrected using both the CamSci sensor located in TRE and the FLIR values obtained when the primary goniometer arm was in the nadir position. First, the FLIR was corrected assuming the CamSci sensor present in the TRE was the correct temperature of the emitter. This correction value was assumed constant throughout the experiment and for all viewing angles and was calculated as an average of the three data points from the nadir arm position. The IR temperature data was corrected in the same way, with the CamSci temperature being subtracted from the average IR temperature and averaged over the three available nadir values. Figure 6.1 is a plot of the difference between corrected FLIR and corrected IR temperature data for all 4 sediments and all nominal temperature settings. The TRE data is also present in this image. It should be noted that nadir data does not necessarily pass through zero for all points; this is due to the fact that an average was applied when calculating the corrected values.

The same trend can be seen in Figure 6.1 that was seen previously in the Raw Data section. The main difference is that the values in Figure 6.1 are closer to the actual temperature of the sediments during the experiment. This data will be useful in future work that will be done analyzing the behavior of sediments over a heating and cooling cycle. Also noteworthy is the fact that the most significant error due to viewing angle and the most consistent data is seen for the nominal temperatures that provide the largest difference between ambient air temperature and sediment temperature. This agrees with previous work done by Cuenca and Sobrino (2004) that stated that in order to avoid residual error there must be a relatively large difference between ambient and sediment temperature.

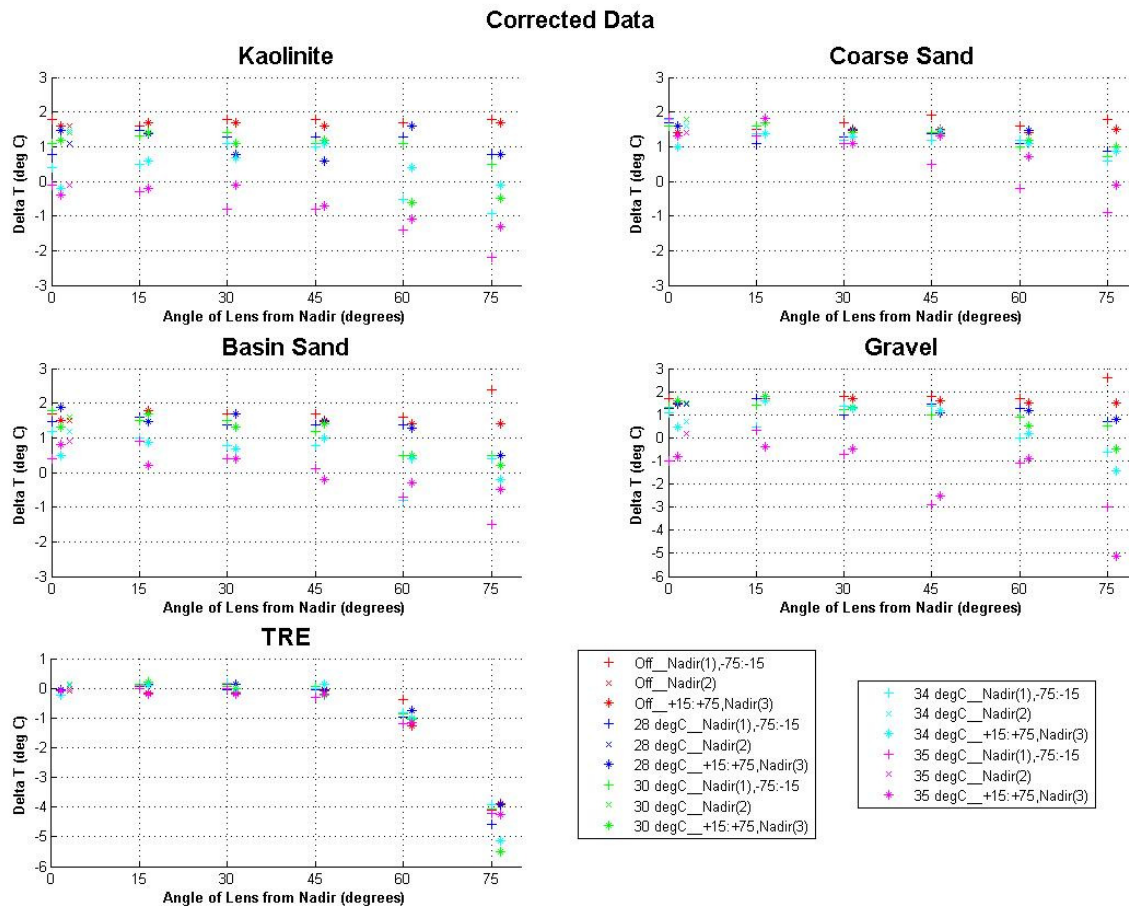


Figure 6.1: Difference between corrected FLIR and corrected IR temperature data for all sediments and temperature ranges.

Chapter 7

CONCLUSIONS

The overall goal of this research is to be able to quantify variations in apparent surface temperature as a function of imager viewing angle. Eventually a database could be built containing unique information for different sediment types (each having a physical properties associated with it) and how they react over a heating and cooling cycle. In order to accomplish this, we must first establish testing procedures that adequately mimic field conditions in a laboratory setting. This small study of variability of apparent surface temperature was successful in doing so. Data collected from these experiments concurs with analyses completed in field experiments, and the testing procedure is repeatable for many different sediments types and combinations. Working off of this research, more accurate data can be collected by obtaining a heating source with less spatio-temporal variations and by further isolating the immediate testing area. Error associated with the single-point infrared thermometer can be avoided by using two thermal imagers; one always at nadir and one collecting images at varying angles. By making small equipment changes, many different sediment types can be analyzed at varying temperature and moisture conditions.

REFERENCES

- Buettner, K. J. K., and C. D. Kern, 1965. The determination of infrared emissivities of terrestrial surfaces, *J. Geophys. Res.*, Vol. 70, pp. 1329-1337
- Cuenca J., & J. A. Sobrino (2004). "Experimental measurements for studying angular and spectral variation of thermal infrared emissivity." *Applied Optics*, Vol. 43, No. 23, pp. 4598-4602
- Cuenca J., J. A. Sobrino, G. Soria (2005). "An experimental study of angular variations of brightness surface temperature for some natural surfaces." *Proceedings of the MERIS (A)ATSR Workshop 2005 (ESA SP-597)*. 26 - 30 September 2005 ESRIN, Frascati, Italy. Editor: H. Lacoste. Published on CDROM., p.33.1
- Sobrino, J.A., and J. Cuenca (1999). "Angular variation of thermal infrared emissivity for some natural surfaces from experimental measurements." *Applied Optics*, Vol. 38, No. 18, pp.3931-3936

APPENDIX A: Soil Classification Data

Fine Sand					
Sieve Number	Wt of Pan (g)	Wt with sample (g)	Wt of Sample (g)	% retained	% passing
4	516	516	0	0%	100%
10	731.1	731.1	0	0%	100%
20	429.5	451.5	22	6%	94%
40	339.5	552.7	213.2	60%	40%
60	360.1	475.2	115.1	89%	11%
100	510.3	549.3	39	99%	1%
140	349.5	351.8	2.3	100%	0%
200	292.8	293.4	0.6	100%	0%
pan	374.5	374.6	0.1	100%	0%
			Total = 392.2		
Coarse Sand					
Sieve Number	Wt of Pan (g)	Wt with sample (g)	Wt of Sample (g)	% retained	% passing
4	516.3	516.3	0	0%	100%
10	482	506.1	24.1	6%	94%
20	436.3	630.1	193.8	53%	47%
40	393.7	578	184.3	97%	3%
60	421.3	432.4	11.1	100%	0%
100	510.2	510.4	0.2	100%	0%
140	306	306	0	100%	0%
200	484.6	484.6	0	100%	0%
pan	490.5	490.5	0	100%	0%
			Total = 413.6		

APPENDIX B: Experiment Data

